Structural effects in $R_{0.5}Sr_{0.5}MnO_3$ perovskites (R = rare earth)

1999 J. Phys.: Condens. Matter 11 8103

(http://iopscience.iop.org/0953-8984/11/41/313)

J. Phys.: Condens. Matter **11** (1999) 8103–8109. Printed in the UK PII: S0953-8984(99)05226-1

Structural effects in $R_{0.5}Sr_{0.5}MnO_3$ perovskites (R = rare earth)

G H Rao†‡, I D Brown§ and K Bärner‡

† Institute of Physics & Centre for Condensed Matter Physics, Chinese Academy of Sciences, Beijing 100080, People's Republic of China

‡ IV. Physikalisches Institut der Universität Göttingen, Bunsenstrasse 11–15, D-37073, Göttingen, Germany

§ Brockhouse Institute for Materials Research, McMaster University, Hamilton, Ontario, Canada L8S 4M1

Received 16 June 1999, in final form 18 August 1999

Abstract. A comprehensive magnetic phase diagram for the perovskites $R_{0.5}Sr_{0.5}MnO_3$ (R = trivalent rare-earth ions) that show an antiferromagnetic (AFM) transition at low temperature, and an A-type layered AFM structure is constructed by using the global instability index, $R1$, as a structural parameter. The phase boundaries are well defined in the phase diagram, indicating that $R1$ is an adequate structural parameter for depicting the structural effects arising from both the cation disorder and size mismatch on the magnetic and electric properties of the perovskite manganites. It is shown that variation of the antiferromagnetic transition temperature, T_N, that occurs upon R^{3+} substitution is different to that on Sr^{2+} substitution; this can be understood in terms of a tuned competition between ferromagnetic and antiferromagnetic interactions. On the basis of bond valence analysis, a neutron diffraction experiment and the transport properties, we propose a novel approach of classifying two types of $R_{0.5}A'_{0.5}MnO_3$ compound (A′ = divalent alkaline-earth ions) according to the magnetic structure, and accordingly the resistivity, of the ground state of a compound. Such a classification reveals a close correlation among the magnetic, crystal structure and transport properties of the compounds. The electronic effects in these two types of compound seem to be different in magnitude and lead to different AFM structures.

1. Introduction

The hole-doped perovskite manganites $R_{1-x}A'_xMnO_3$ (R = trivalent rare-earth ions; A′ = divalent alkaline-earth ions) exhibit the simultaneous occurrence of ferromagnetism and metallic conductivity at an appropriate doping level, which can be understood on the basis of double-exchange (DE) interaction between the spins of Mn^{3+} and Mn^{4+} ions via hopping of the Mn e_g electrons: e_g(Mn)–2pσ(O)–e_g(Mn), and a strong Hund's coupling between the Mn t_{2g}^3 and the e_g electrons [1–3]. $R_{1-x}A'_xMnO_3$ usually shows a maximum Curie temperature and colossal magnetoresistance (CMR) at $x \approx 0.3$ [4–6]. In competition with the ferromagnetic DE interaction, there exist many other instabilities such as antiferromagnetic superexchange between the t_{2g}^3 electrons via the π-orbits: t_{2g}(Mn)–2pπ(O)–t_{2g}(Mn), and Jahn–Teller, orbit-ordering and charge-ordering interactions in the perovskite manganites. Charge-ordering transitions, i.e., real-space ordering of the doped holes, have been proposed to occur in many $R_{1-x}A'_xMnO_3$ compounds with $x \approx 0.5$ [7–9]. The charge-ordering transition is well known in transition metal oxides; e.g. Fe_3O_4 exhibits a spatial ordering of the Fe^{3+} and Fe^{4+} ions at ∼120 K [10], and is associated with a narrow conduction band and a large Coulomb energy that overcomes the kinetic energy of electric carriers.

0953-8984/99/418103+07$30.00

Moritomo *et al* classified two kinds of charge-ordering compound in the $R_{0.5}A'_{0.5}MnO_3$ family on the basis of magnetic measurements [11]. One of them (type I) is exemplified by $Nd_{0.5}Sr_{0.5}MnO_3$, in which a ferromagnetic metallic state ($T_C \sim 250$ K) gives way to an antiferromagnetic charge-ordering state at around 150 K ($T_{CO} = T_N$). The other (type II) is exemplified by $Pr_{1-x}Ca_xMnO_3$ ($0.3 \leqslant x \leqslant 0.5$), in which an insulating charge ordering occurs in the paramagnetic region at T_{CO} ($\sim$200 K) and an antiferromagnetic spin ordering takes place at a lower temperature ($T_N \approx 140$ K). Type II compounds are thought to be associated with a narrower one-electron bandwidth (W) than type I compounds. Electron diffraction reveals superlattice spots due to the charge ordering in $La_{0.5}Ca_{0.5}MnO_3$ [12]. The charge-ordering compounds exhibit a CE-type antiferromagnetic structure below T_N (in the nomenclature of Goodenough [4]). In this classification, both $Nd_{0.5}Sr_{0.5}MnO_3$ and $Pr_{0.5}Sr_{0.5}MnO_3$ are assigned as type I charge-ordering compounds. $Pr_{0.5}Sr_{0.5}MnO_3$ shows $T_C \approx 270$ K and $T_{CO} = T_N \approx 140$ K [8, 13, 14]. However, recent neutron diffraction study revealed that $Pr_{0.5}Sr_{0.5}MnO_3$ exhibits an A-type layered antiferromagnetic (AFM) structure below T_N without a clear sign of long-range charge ordering, while $Nd_{0.5}Sr_{0.5}MnO_3$ has the CE-type AFM structure with charge ordering [15]. The difference in the AFM structure is thought to be responsible for the difference in electric transport properties, i.e. the resistivity of the A-type AFM state is much lower than that of the CE-type AFM state. Electronic structure calculation indicated that the CE-type AFM state is stabilized by a strong Jahn–Teller distortion, while the A-type AFM state is stabilized by the in-plane breathing-type lattice distortion [16].

In addition to the hole doping level, it is well known that the double-exchange interaction in the perovskite manganites is highly sensitive to lattice effects. One of the lattice effects results from the size mismatch between Mn and the average size of R and A′ cations, traditionally measured by the Goldschmidt tolerance factor, $t = (r_A + r_O)/\sqrt{[2(r_B + r_O)]}$, for a perovskite ABO_3. For most of the CMR perovskite manganites, $t < 1$, which implies that the cage formed by corner-sharing MnO_6 octahedra is on average too large for the cations at the A sites, and the structure is expected to distort by twisting and tilting the MnO_6 octahedra cooperatively [17]. Such a structural distortion leads to a bending of the Mn–O–Mn bonds, a reduction of the effective one-electron bandwidth (W) and a weakening of the DE interaction [18]. Another lattice effect can be attributed to the size and charge difference between the R^{3+} and A'^{2+} cations randomly distributed over the A sites, i.e. cation disorder, which will cause inhomogeneity in the background potential experienced by the e_g electrons when they move through the crystal and give rise to some regions of low potential in which the electrons can be trapped. The latter effect may become significant in many perovskite manganites and cannot be described by the tolerance factor—equivalently $\langle r_A \rangle$ at a fixed doping level [19, 20]. Attfield *et al* suggested using the variance of the ionic radius distribution of A-site cations, σ^2, in combination with $\langle r_A \rangle$ to characterize the lattice effects in perovskite-type oxides [19, 21]. They observed a linear correlation between the metal–insulator (M–I) transition temperature $T_m(\langle r_A \rangle, \sigma^2)$ and σ^2 at a fixed $\langle r_A \rangle$: $T_m(\langle r_A \rangle, \sigma^2) = T_m(\langle r_A \rangle, 0) - p_1\sigma^2$ for $R_{0.7}A'_{0.3}MnO_3$ when σ^2 is not too large. $T_m(\langle r_A \rangle, 0)$ is an extrapolated M–I transition temperature for $R_{0.7}A'_{0.3}MnO_3$ without cation-size disorder at $\langle r_A \rangle$. A smooth and monotonic relationship between $T_m(\langle r_A \rangle, 0)$ and $\langle r_A \rangle$ for $R_{0.7}A'_{0.3}MnO_3$ was established. Damay *et al* also found that the parameter $\langle r_A \rangle$ alone cannot properly characterize the magnetic properties of $R_{0.5}A'_{0.5}MnO_3$ [13]. They followed the approach of Attfield *et al* in analysing their experimental data, but failed to obtain an unambiguous relation between the hypothetical Curie temperature $T_C(\langle r_A \rangle, 0)$ of $R_{0.5}A'_{0.5}MnO_3$ and $\langle r_A \rangle$, which was attributed to the complex magnetic properties of the compounds. A projection onto the $\langle r_A \rangle$–σ^2 plane of the T_C–$\langle r_A \rangle$–σ^2 magnetic phase diagram was given for $R_{0.5}A'_{0.5}MnO_3$ in reference [13], which unfortunately provides little information about the relation between T_C and the structural parameters ($\langle r_A \rangle$, σ^2).

On the basis of the bond valence model [17], we proposed in an earlier letter using the global instability index, $R1$, as a single structural parameter to characterize the static lattice effects in $R_{0.7}A'_{0.3}MnO_3$ [22]. The magnetic phase diagram giving T_C (or T_m) versus $R1$ for $R_{0.7}A'_{0.3}MnO_3$ reveals well defined phase boundaries. The calculation of $R1$ is as simple as that of $\langle r_A \rangle$, but it seems to include in an implicit way the contributions of both $\langle r_A \rangle$ and σ^2 to the lattice effects. In this paper we apply our approach to analyse the magnetic and electric properties of $R_{0.5}A'_{0.5}MnO_3$ compounds. The experimental data, which were derived from low-field magnetization measurements on about 50 different compounds, from the reports of the same laboratory, are used in the analysis [13, 14]. These compounds exhibit an FM–AFM transition and a low-temperature resistivity of the same order of magnitude as that of $Pr_{0.5}Sr_{0.5}MnO_3$. A comprehensive magnetic and electronic phase diagram showing the relation between the magnetic transition temperature and $R1$ is achieved.

2. Characterization of structural effects

The details of the approach have been presented in our earlier letter [22]. The essential stage of the approach is the construction of a reference structure, so that the relative stability of real compounds can be compared. We constructed an ideal cubic perovskite manganite as the reference structure, in which all of the Mn–O bonds are of the same length and unstrained, and the Mn–O–Mn angles are either 90 or 180 degrees. This corresponds to a situation in which the Mn^{3+} and Mn^{4+} ions distribute randomly over Mn sites with an average charge (+3.3 for $x = 0.3$ and +3.5 for $x = 0.5$) and exactly obey the bond valence sum rule [17]. There are no adjustable atomic position parameters in the reference structure and its lattice parameter as well as the Mn–O and (R, A′)–O bond lengths can be determined from the bond valence of the Mn–O bond and the relation between the bond valence and bond length. For $x = 0.5$, the Mn–O bond length d_{Mn-O} is 1.956 Å, and therefore the cubic lattice parameter of the reference structure is 3.912 Å, and the A–O bond length d_{A-O} is 2.766 Å regardless of the nature of A. Such a reference structure can simplify the calculation of $R1$ without altering the relative order of the values of $R1$ for different compounds. In fact the calculation of the Goldschmidt tolerance factor also uses a reference structure in which rigid ions are close packed in an ideal cubic perovskite.

Suppose a compound $R_{0.5}A'_{0.5}MnO_3$ adopts the reference structure; one can define the global instability index of the structure [17, 23]:

$$R1 = \langle d_i^2 \rangle^{1/2} \tag{1}$$

where the average is taken over all ions in a unit cell, d_i is the difference between the chemical valence of ion i, V_i, and the sum of the bond valences around this ion:

$$d_i = V_i - \sum_j s_{ij} \tag{2}$$

and the bond valence s_{ij} of a chemical bond is related to its length R_{ij} by

$$s_{ij} = \exp\left(\frac{R_0 - R_{ij}}{B}\right) \tag{3}$$

where $B = 0.37$ and R_0 is the length of a bond of unit valence. The values of R_0 for most of the common bonds are tabulated in reference [24]. The values of R_0 used in the present work for calculating the valence of the bond between a cation and an oxygen are listed in table 1. d_i is computed according to equations (2) and (3) by placing ion i at the corresponding site in the reference structure, i.e. Mn ions at B sites and R or A′ ions at A sites. The calculated d_i are

Table 1. The values of R_0 used in this work for the bond between a cation and oxygen, and the values of d_i for the ions in the ideal perovskite structure.

Ions	La^{3+}	Pr^{3+}	Sm^{3+}	Gd^{3+}	Y^{3+}	Ca^{2+}	Sr^{2+}	Ba^{2+}	Mn^{3+}	Mn^{4+}
R_0	2.172	2.138	2.090	2.058	2.019	1.967	2.118	2.285	1.760	1.753
d_i	0.591	0.803	1.070	1.230	1.407	0.616	−0.082	−1.270	0	0

also listed in table 1. As we assumed in constructing the reference structure, $d_{\mathrm{Mn}} = 0$, so $d_{\mathrm{O^{2-}}}$ can be easily derived from the values of d_i of A-site ions according to electronic neutrality of the compound [22]:

$$d_{\mathrm{O^{2-}}} = [(1 - x)d_{\mathrm{R^{3+}}} + x d_{\mathrm{A'^{2+}}}]/3.$$

Therefore, the calculation of $R1$ is as simple as that of a tolerance factor that can be derived from the tabulated data for a given compound $R_{0.5}A'_{0.5}MnO_3$.

Within the framework of the bond valence model, larger values of $R1$ and d_i are indicative of strained bonds which can lead to instability in the crystal structure. $R1$ provides a measure indicating the tendency towards structural distortion in a perovskite manganite if it adopts the reference structure. Equivalently $R1$ is a measure of the magnitude of the distortion taking place in a real structure of the compound. In the same way, d_i^2 is a measure of local lattice distortion around ion i in the compound [25]. It must be pointed out that the construction of the reference structure and the calculation of $R1$ do not take into account the electronic effects, such as the Jahn–Teller effect, which may be significant for perovskite manganates. However, if the contribution of the electronic effects is small or comparable for the compounds investigated [26], $R1$ given in present paper can still serve to order the compounds in a way that indicates which compound will be more likely to distort.

3. Results and discussion

Figure 1 shows the dependence of the magnetic transition temperatures, T_C and T_N, on the global instability index $R1$ of $R_{0.5}A'_{0.5}MnO_3$. Five phase regions are clearly distinguishable. In contrast to the case for the phase diagrams reported in reference [13], the data for both R-ion- and A′-ion-substituted compounds can be mapped onto figure 1 consistently, and the T_C-values nicely define the corresponding phase boundaries. As $R1$ increases, the lattice distortion and the bending of the Mn–O–Mn bonds increase, leading to a weakening of the double exchange and a reduction of T_C. In $R_{0.7}A'_{0.3}MnO_3$, the ferromagnetic metallic (FMM) state becomes unstable when $R1 \gtrsim 0.47$ v.u. (valence units) [22], while it is unstable when $R1 \gtrsim 0.34$ v.u. for $R_{0.5}A'_{0.5}MnO_3$, implying that the double-exchange interaction in the latter is indeed weaker than that in the former and that the FMM state in the latter accommodates smaller lattice distortions. The comprehensive magnetic and electronic phase diagram shown in figure 1 indicates that our approach is appropriate for $R_{0.5}A'_{0.5}MnO_3$ compounds, although their magnetic properties are more complex than those of $R_{0.7}A'_{0.3}MnO_3$.

It is interesting to note that the AFM state occurs exclusively in a limited range of $R1$ from ∼0.235 v.u. to ∼0.345 v.u. Taking into account that a stable spin arrangement results from a competition of the ferromagnetic DE interaction with other interactions, on the one hand, and that both the DE exchange coupling J_{FM} and antiferromagnetic exchange coupling J_{AFM} decrease with the increase of the bending of the Mn–O–Mn bonds, on the other hand [26], we see that small $R1$ implies small lattice distortions that benefit the DE exchange, leading to a suppression of the AFM state, while large $R1$ is associated with larger lattice distortions,

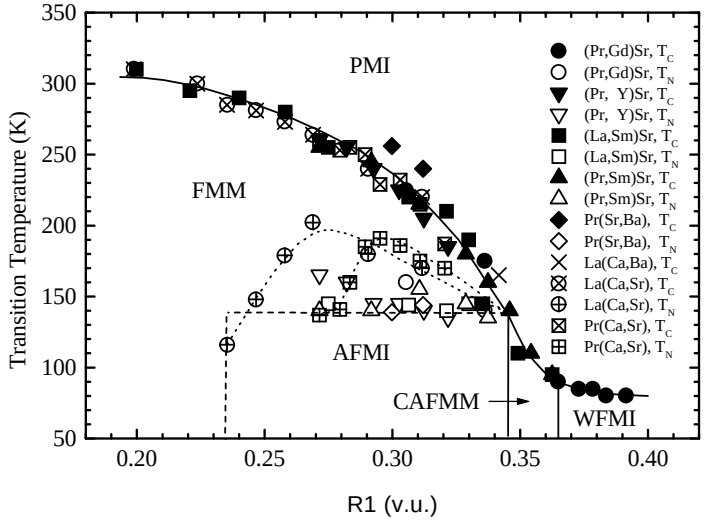

Figure 1. The magnetic and electronic phase diagram of $R_{0.5}A'_{0.5}MnO_3$. The lines are guides to the eyes. The phase regions are assigned after reference [14]: PMI—paramagnetic insulator; FMM—ferromagnetic metal; AFMI—antiferromagnetic insulator; CAFMM—canted antiferromagnetic metal; WFMI—weak ferromagnetic insulator. The labels (Gd, Pr)Sr and Pr(Ba, Sr) etc represent $(Gd, Pr)_{0.5}Sr_{0.5}MnO_3$ and $Pr_{0.5}(Ba, Sr)_{0.5}MnO_3$ etc.

and accordingly a large bending of Mn–O–Mn bonds; the reductions of both J_{FM} and J_{AFM} and the subtle competition between FM and AFM interactions can destabilize the AFM state, leading to the canted antiferromagnetic metallic (CAFMM) or weak ferromagnetic insulating (WFMI) state for large $R1$, as shown in figure 1.

Another intriguing feature revealed in figure 1 is that the substitutions for R^{3+} and Sr^{2+} give rise to different effects on T_N. While the substitution for R^{3+} changes T_N slightly, the substitution for Sr^{2+} results in a maximum T_N. Nevertheless, all the T_N–$R1$ curves converge at $R1 \approx 0.34$ v.u. As listed in table 1, $d_{Sr^{2+}} = -0.082$ v.u., which means that the Sr^{2+} ion fits the A-site cage in the reference structure nicely and the local lattice distortions around Sr^{2+} ions are negligible. Therefore the local environment around Sr^{2+} favours the hopping of the e_g electrons and the DE interaction. Since the A-type AFM state can be regarded as resulting from a subtle competition between ferromagnetic DE and antiferromagnetic superexchange interactions, and the DE interaction persists on the FM layers, the fractional Sr^{2+} content can play a crucial role as regards a stable spin configuration. Substitution for Sr^{2+} ions with smaller divalent ions (e.g. Ca^{2+}) reduces the Sr content and the associated regions, benefiting the DE interaction, stabilizing the AFM state and giving rise to a higher T_N. In conjunction with the effects of the bending of Mn–O–Mn bonds on J_{FM} and J_{AFM}, the substitution for Sr^{2+} can lead to the maximum T_N. In contrast; substitution for R^{3+} does not reduce the Sr^{2+} content; the substitution effects are attributed essentially to the bending of Mn–O–Mn bonds which reduces both J_{FM} and J_{AFM}. This plausible explanation seems to be further evidenced by the substitution effect of a small amount of Ba^{2+} for Sr^{2+}. Since $d_{Ba^{2+}} = -1.27$ v.u. (see table 1), the A-site cage in the reference structure is too small for Ba^{2+} and the local lattice distortions around Ba^{2+} are caused by slightly stretching the Mn–O bonds [17]. Therefore, the substitution of Ba^{2+} for Sr^{2+} does not change the number of bending Mn–O–Mn bonds. Experimentally, $Pr_{0.5}Sr_{0.5-x}Ba_{0.5}MnO_3$ ($x < 0.2$) shows the FM–AFM transition at ∼140 K, which is close to T_N for the R-ion-substituted compounds.

It is noteworthy that the data shown in figure 1 are essentially those for $La_{0.5}Sr_{0.5}MnO_3$- and $Pr_{0.5}Sr_{0.5}MnO_3$-based compounds, which exhibit relatively low resistivity at low temperature. $La_{0.5}Sr_{0.5}MnO_3$ exhibits a FM ground state, and a FM–AFM transition can be introduced as $R1$ increases by ion substitution. Although $Pr_{0.5}Sr_{0.5}MnO_3$ undergoes a FM–AFM transition at low temperature, neutron diffraction reveals no clear sign of a long-range charge ordering in the AFM state and the AFM phase crystallizes in an A-type layered structure with a relatively small Jahn–Teller distortion [15]. In contrast, $Nd_{0.5}Sr_{0.5}MnO_3$ and $R_{0.5}Ca_{0.5}MnO_3$ (R = La, Pr, Nd, Sm) exhibit the CE-type AFM structure with a high resistivity and a well defined charge-ordering transition at T_{CO} ($\geqslant T_N$). Electronic structure calculations reveal that the CE-type AFM state is associated with strong Jahn–Teller distortions [16]. For a real structure the global instability index, when calculated from the observed bond lengths, characterizes the lattice distortions arising from both the geometric effects such as size mismatch and the electronic effects such as the Jahn–Teller effect. However, the construction of the reference structure and the definition of $R1$ according to equation (1) do not take into account the electronic effects, and therefore $R1$ given in the present work cannot be used to order compounds with different strengths of electronic effects. In fact, $Nd_{0.5}Sr_{0.5}MnO_3$ ($R1 = 0.335$ v.u.) shows a T_C of 255 K [7], which is much higher than the prediction of figure 1 and implies that the lattice distortion due to the geometric effects in $Nd_{0.5}Sr_{0.5}MnO_3$ is smaller than that measured by $R1$. In other words, the electronic effects are larger in $Nd_{0.5}Sr_{0.5}MnO_3$ than in the compounds shown in figure 1, which is consistent with their AFM structures as revealed by neutron diffraction [15] and band-structure calculations [16]. The successful construction of figure 1 seems to indicate that the electronic effects in the compounds investigated are small or comparable, as assumed by Kumar and Rao [26].

On the basis of the bond valence analysis, the neutron diffraction experiment and transport properties, it is reasonable to suggest the alternative approach of classifying two types of $R_{0.5}A'_{0.5}MnO_3$ compound according to the magnetic structure of the ground state of the compound. Type I consists of most of the Sr-doped compounds, $R_{0.5}Sr_{0.5}MnO_3$, which show an FM or an A-type layered AFM ground state with low resistivity. Another type (type II) includes $Nd_{0.5}Sr_{0.5}MnO_3$ and Ca-doped compounds, $R_{0.5}Ca_{0.5}MnO_3$, which exhibit a well defined charge-ordering transition ($T_C > T_N$) and the CE-type AFM ground state with high resistivity. Such a classification reveals a close correlation among the magnetic, crystal structure and transport properties. Bond valence analysis and band-structure calculation seem to indicate that the electronic effects in these two types of compound are different in magnitude and responsible for the different AFM structures.

4. Concluding remarks

In conclusion, we construct a well defined and comprehensive magnetic and electronic phase diagram for $R_{0.5}A'_{0.5}MnO_3$, which shows an A-type AFM state at low temperature, by using the global instability index $R1$ as a single chemical parameter. The success in constructing the phase diagrams of $R_{1-x}A'_xMnO_3$ with $x = 0.3$ and $x = 0.5$ indicates that $R1$ is indeed a better structural parameter than either $\langle r_A \rangle$ or σ^2 for depicting the lattice effects in the perovskite manganites. It seems reasonable to suggest a novel way to classify two types of $R_{0.5}A'_{0.5}MnO_3$ compound—according to the magnetic structure of the ground state of the compound; this reveals a close correlation among magnetic, crystal structure and transport properties. The electronic effects in these two types of compound are different in magnitude and responsible for different magnetic structures of the ground state.

Acknowledgments

GHR is indebted to Alexander von Humboldt (AvH) Foundation for a Research Fellowship. IDB wishes to thank the Natural Science and Engineering Council of Canada for financial support. KB wishes to acknowledge the continuing support of the Deutsche Forschungsgemeinschaft (DFG).

References

[1] Zener C 1951 *Phys. Rev.* **82** 403
[2] Anderson P W and Hasegawa H 1955 *Phys. Rev.* **100** 675
[3] de Gennes P-G 1960 *Phys. Rev.* **118** 141
[4] Goodenough J B 1955 *Phys. Rev.* **100** 564
[5] Jin S, Tiefel T H, McCormack M, Fastnacht R A, Ramesh R and Chen L H 1994 *Science* **264** 413
[6] Rao G H, Sun, J R, Kattwinkel A, Haupt L, Bärner K, Schmitt E and Gmelin G 1999 *Physica* B **269** 379
[7] Kuwahara H, Tomioka Y, Asamitsu A, Moritomo Y and Tokura Y 1995 *Science* **270** 961
[8] Tomioka Y, Asamitsu A, Moritomo Y, Kuwahara H and Tokura Y 1995 *Phys. Rev. Lett.* **74** 5108
[9] Tokura Y, Kuwahara H, Moritomo Y, Tomioka Y and Asamitsu A 1996 *Phys. Rev. Lett.* **76** 3184
[10] Verwey E J W, Haaymann P W and Romejin F C 1947 *J. Chem. Phys.* **15** 181
[11] Moritomo Y, Kuwahara H, Tomioka Y and Tokura Y 1997 *Phys. Rev.* B **55** 7549
[12] Chen C H and Cheong S-W 1996 *Phys. Rev. Lett.* **76** 4042
[13] Damay F, Martin C, Maignan A and Raveau B 1997 *J. Appl. Phys.* **82** 6181
[14] Damay F, Maignan A, Martin C and Raveau B 1997 *J. Appl. Phys.* **81** 1372
[15] Kawano H, Kajimoto R, Yoshizawa H, Tomioka Y, Kuwahara H and Tokura Y 1997 *Phys. Rev. Lett.* **78** 4253
[16] Mizokawa T and Fujimori A 1997 *Phys. Rev.* B **56** R493
[17] Brown I D 1992 *Acta Crystallogr.* B **48** 553
[18] Archibald W, Zhou J-S and Goodenough J B 1996 *Phys. Rev.* B **53** 14 445
[19] Rodriguez-Martinez L M and Attfield J P 1996 *Phys. Rev.* B **54** R15 622
[20] Sun J R, Rao G H and Liang J K 1997 *Appl. Phys. Lett.* **70** 1900
[21] Attfield J P 1998 *Chem. Mater.* **10** 3239
[22] Rao G H, Bärner K and Brown I D 1998 *J. Phys.: Condens. Matter* **10** L757
[23] Sanches-Salinas A, Garcia-Munoz J L, Rodriguez-Carvajal J, Saez-Puche R and Martinez J L 1992 *J. Solid State Chem.* **100** 201
[24] Brown I D and Altermatt D 1985 *Acta Crystallogr.* B **41** 244
[25] Rao G H, Sun J R, Liang J K and Zhou W Y 1997 *Phys. Rev.* B **55** 3742
[26] Kumar N and Rao C N R 1997 *J. Solid State Chem.* **129** 363